Korean Journal of Radiology

KJR

Accelerated Time-of-Flight Magnetic Resonance Angiography with Sparse Undersampling and Iterative Reconstruction for the Evaluation of Intracranial Arteries

Hehan Tang, MS[1], Na Hu, MD[1], Yuan Yuan, MS[1], Chunchao Xia, BS[1], Xiumin Liu, BS[1], Panli Zuo, PhD[2], Aurelien F. Stalder, PhD[3], Michaela Schmidt, PhD[4], Xiaoyue Zhou, PhD[3], Bin Song, MD[1], Jiayu Sun, MD[1]

[1]Department of Radiology, West China Hospital of Sichuan University, Chengdu, China; [2]MR Collaboration NEA, Siemens Healthineers Ltd., Beijing, China; [3]MR Collaboration NEA, Siemens Healthineers Ltd., Shanghai, China; [4]Siemens Healthineers GmbH, Erlangen, Germany

Objective: To compare the image quality of three-dimensional time-of-flight (TOF) magnetic resonance angiography (MRA) with sparse undersampling and iterative reconstruction (sparse TOF) with that of conventional TOF MRA.

Materials and Methods: This study included 56 patients who had undergone sparse TOF MRA for intracranial artery evaluation on a 3T MR scanner. Conventional TOF MRA scans were also acquired from 29 patients with matched acquisition times and another 27 patients with matched scanning parameters. The image quality was scored using a five-point scale based on the delineation of arterial vessel segments, artifacts, overall vessel visualization, and overall image quality by two radiologists independently, and the data were analyzed using the non-parametric Wilcoxon signed-rank test. Contrast ratios (CRs) of vessels were compared using the paired t test. Interobserver agreement was calculated using the kappa test.

Results: Compared with conventional TOF at the same spatial resolution, sparse TOF with an acceleration factor of 3.5 could reduce acquisition time by 40% and showed comparable image quality. In addition, when compared with conventional TOF with the same acquisition time, sparse TOF with an acceleration factor of 5 could also achieve higher spatial resolution, better delineation of vessel segments, fewer artifacts, higher image quality, and a higher CR ($p < 0.05$). Good-to-excellent interobserver agreement (κ: 0.65–1.00) was obtained between the two radiologists.

Conclusion: Compared with conventional TOF, sparse TOF can achieve equivalent image quality in a reduced duration. Furthermore, using the same acquisition time, sparse TOF could improve the delineation of vessels and decrease image artifacts.

Keywords: *Time-of-Flight (TOF); Magnetic resonance angiography (MRA); Intracranial vessels; Sparse; Iterative reconstruction*

INTRODUCTION

Time-of-flight (TOF) magnetic resonance angiography (MRA) is a non-invasive, non-contrast-enhanced MRA technique that provides contrast between vessels and stationary tissues by inducing blood inflow effects (1-

4). Three-dimensional (3D) TOF MRA with multiple slabs is performed widely to depict the cerebral vasculature in the diagnosis of cerebral vascular pathologies such as intracranial occlusions, intracranial aneurysm, and arteriovenous malformations (5,6). However, conventional TOF techniques suffer from relatively long acquisition times

for images with high spatial resolution and large coverage, which often require longer than 5 minutes. Parallel imaging techniques such as generalized autocalibrating partially parallel acquisitions (GRAPPA) and modified sensitivity encoding (mSENSE) allow imaging acceleration by a factor of 2–3, but further reduction of the acquisition time is challenging because of the reduced signal-to-noise ratio (SNR) (7, 8).

To overcome this limitation, sparse methods, which exploit known sparsity properties of the data in transform domains, in combination with incoherent k-space sampling and non-linear reconstruction algorithms were recently proposed to further accelerate the acquisition speed in magnetic resonance imaging (MRI) (9-11). Because of the intrinsic sparsity of the pixel domain and high contrast-to-noise ratio, contrast-enhanced and non-contrast-enhanced MRA are excellent candidates for sparse methods (12-14). However, because of the long reconstruction times and often off-line reconstructions, the clinical application and evaluation of sparse methods remain limited (12, 15). In this context, a sparse TOF MRA using sparse methods with inline iterative reconstruction on a standard clinical system has been suggested recently (16, 17) and applied to cerebral aneurysms (18).

The purpose of this study was to prospectively compare the image quality of 3D sparse TOF MRA with incoherent sampling and iterative reconstruction with that of conventional TOF MRA in a clinical setting and on a standard clinical MR system.

MATERIALS AND METHODS

Subjects

This study was approved by the local Institutional Review Board and written informed consent was obtained from all patients. A total number of 56 patients with dizziness (33 males and 23 females; mean age, 53.4 ± 18.6 years) were enrolled in this study between March 2017 and July 2017.

MRI

The MRI examination was performed on a 3T magnetic resonance (MR) scanner (MAGNETOM Skyra, Siemens Healthineers, Erlangen, Germany) with a 20-channel phased array head-neck coil for evaluation of the intracranial arteries. To compare the image qualities of sparse and conventional TOF MRA, all patients were divided into two groups (Table 1) to be examined by prototype sparse and conventional TOF sequences with 1) nearly matched acquisition times and 2) nearly matched spatial resolutions using the acquisition parameters shown in Table 2.

Table 1. Clinical Characteristic of Subjects

Parameters	TOF and Sparse TOF with Same Resolution	TOF and Sparse TOF with Same Scan Time
Number of patients	27	29
Age (years)	48.6 ± 18.3	57.8 ± 18.0
Sex (male/female)	16/11	17/12

Sparse TOF = TOF with sparse undersampling and iterative reconstruction, TOF = time-of-flight

Table 2. MRI Parameters of TOF and Sparse TOF

Parameter	TOF and Sparse TOF with Same Resolution		TOF and Sparse TOF with Same Scan Time	
	TOF	Sparse TOF	TOF	Sparse TOF
TE/TR (ms)	3.43/21	3.43/21	3.43/21	3.43/21
FOV (mm^2)	200 x 180	200 x 180	200 x 180	200 x 180
Voxel size (interpolated, mm^3)	0.3 x 0.3 x 0.4	0.3 x 0.3 x 0.4	0.3 x 0.3 x 0.6	0.3 x 0.3 x 0.4
Slices per slab	56	56	36	60
Slabs	4	4	4	4
Slab distance factor (%)	-19.6	-19.6	-16.7	-16.7
Acceleration method	GRAPPA	Sparse sampling	GRAPPA	Sparse sampling
Acceleration factor	2	3.5	3	5
Partial fourier	7/8	NA	7/8	NA
TA (min)	6:32	4:10	3:44	3:52

FOV = field of view, GRAPPA = generalized autocalibrating partially parallel acquisition, NA = not applicable, TA = acquisition time, TE = echo time, TR = repetition time

Image Sampling and Reconstruction

For the conventional TOF sequence, a GRAPPA parallel imaging technique with an accelerator factor of 2 or 3 was applied along the phase-encoding (left-right) direction. A slice partial Fourier value of 7/8 was used in the image acquisition. For the sparse TOF prototype sequence, each slab was acquired using a variable-density Poisson disk sampling pattern in the $k_y - k_z$ phase-encoding plane (17-22) with acceleration factors of 3.5 and 5.

Image reconstruction was performed using a redundant Haar wavelet-based L1-regularized iterative SENSE algorithm with fast iterative shrinkage and a thresholding algorithm (FISTA) integrated inline on the clinical scanner (17, 23). More specifically, it was achieved by solving the following minimization problem:

$$\min_{x}\left\{ \frac{1}{2}\|y - Fx\|_2^2 + \lambda\|W_x\|_1 \right\},$$

where x is the reconstructed image, y is the undersampled k-space data, F is the undersampled Fourier operator, and W and λ represent the redundant Haar wavelet transform and normalized regularization weighting factor, respectively. The number of FISTA iterations was set to 10 and the regularization weighting factor λ was set to 0.008 for sparse TOF acquisition according to a previous report (12). The total image reconstruction time was about 5 minutes. Afterward, sparse TOF images acquired with net acceleration factors of 3.5 and 5 were compared with conventional TOF images acquired using GRAPPA acceleration factors of 2 and 3, respectively. Both the image sampling and reconstruction were carried out on the scanner.

Image Analysis

Image evaluation was performed on a standard post-processing workstation by two neuroradiologists (with 5 and 26 years of experience) who were blinded to the acquisition parameters and patients' information. For the qualitative analysis, the delineation of the vessels was assessed using a five-point grading scale (5-the display of vessels was excellent and with sharp borders; 4-the display of vessels was good and with clear borders; 3-the display of vessels was moderate and with visible borders; 2-the display of vessels was poor with dim borders and affected the diagnosis; and 1-the display of vessels was unclear and could not be diagnosed). The vessels that were used for evaluation included the main branch, primary sub-branch,

and secondary sub-branch of the anterior cerebral artery (ACA), middle cerebral artery (MCA), posterior cerebral artery (PCA), anterior communicating artery (ACoA), posterior communicating artery (PCoA), internal carotid artery (ICA), and basilar artery (BA). The artifacts, overall vessel visualization, and overall image quality were also assessed using a five-point grading scale. The detailed evaluation standards are listed as follows:

1) Artifacts: 5-no artifact; 4-slight aliasing/blurring artifacts that did not affect the diagnosis; 3-a few aliasing/blurring artifacts and slight motion artifacts (the images could be diagnosed); 2-some aliasing/blurring artifacts and significant motion artifacts (artifacts affecting the diagnosis moderately); and 1-severe artifacts (the images could not be diagnosed).

2) Overall vessel visualization: 5-the display of all above-mentioned vessels was excellent; 4-the display of the main and primary branches was good and the secondary branches were visible; 3-the display of the main and primary branches was good but the secondary branches were barely visible; 2-the display of the main branches was good but the primary vessels were barely visible; and 1-the main branches were visible but the primary branches were invisible.

3) Overall image quality: 5-the display of vessels was excellent, sharp, and without artifacts; 4-the display of vessels was good with clear borders and slight artifacts; 3-the display of vessels was moderate with visible borders and a few artifacts, (diagnostic image quality); 2-the display of vessels was poor with blurry borders and some artifacts (image quality moderately affected the diagnosis); and 1-the display of vessels was unclear with severe artifacts (non-diagnostic image quality).

For the quantitative measurement, the signal intensities (SIs) of the vessels and static background tissue were measured on original images and maximum intensity projection (MIP) images to calculate the contrast ratio (CR) as

$$CR = (SI_{vessel} - SI_{background}) / (SI_{vessel} + SI_{background})$$

where SI_{vessel} is the SI of the vessels and $SI_{background}$ is the SI of the static background tissue (24). Regions of interest (ROIs) were placed in the same position on sparse and conventional TOF MRA images from each patient on the proximal left M1 segment of the MCA and the adjacent gray matter. The sizes of the ROIs varied slightly to account for anatomical variations and to maximize ROI size without including voxels from other tissues.

Table 3. Averaged Readers' Scores of TOF and Sparse TOF

Parameter	TOF and Sparse TOF with Same Resolution		TOF and Sparse TOF with Same Scan Time	
	TOF	Sparse TOF	TOF	Sparse TOF
ACA				
Main branch				
R1	4.9 ± 0.4	4.9 ± 0.4	4.8 ± 0.4	5.0 ± 0.0*
R2	4.8 ± 0.5	4.9 ± 0.5	4.8 ± 0.4	5.0 ± 0.0*
κ	0.84	0.65	0.89	1.00
Primary				
R1	4.7 ± 0.7	4.7 ± 0.5	4.5 ± 0.6	4.9 ± 0.3**
R2	4.6 ± 0.7	4.8 ± 0.5	4.4 ± 0.6	4.9 ± 0.3**
κ	0.91	0.89	0.87	0.78
Secondary				
R1	3.6 ± 1.0	3.3 ± 0.9	2.8 ± 1.2	3.8 ± 1.4**
R2	3.6 ± 0.9	3.4 ± 0.9	2.7 ± 1.0	3.9 ± 1.4**
κ	0.84	0.89	0.81	0.89
MCA				
Main branch				
R1	4.9 ± 0.6	4.9 ± 0.3	4.9 ± 0.3	5.0 ± 0.2
R2	4.8 ± 0.6	4.9 ± 0.3	4.9 ± 0.3	5.0 ± 0.2
κ	0.84	0.78	0.78	1.00
Primary				
R1	4.9 ± 0.6	4.9 ± 0.4	4.9 ± 0.3	4.9 ± 0.3
R2	4.8 ± 0.6	4.9 ± 0.5	4.8 ± 0.4	5.0 ± 0.2
κ	0.79	0.65	0.87	0.65
Secondary				
R1	4.3 ± 0.9	4.3 ± 0.8	3.5 ± 0.8	4.3 ± 0.7**
R2	4.2 ± 0.9	4.3 ± 0.8	3.5 ± 0.8	4.3 ± 0.7**
κ	0.94	0.94	0.95	0.89
PCA				
Main branch				
R1	4.9 ± 0.6	5.0 ± 0.2	4.6 ± 0.6	4.8 ± 0.4
R2	4.8 ± 0.8	4.9 ± 0.3	4.7 ± 0.5	4.9 ± 0.3
κ	0.65	0.65	0.78	0.87
Primary				
R1	4.8 ± 0.6	4.7 ± 0.4	3.3 ± 1.0	4.5 ± 0.7**
R2	4.7 ± 0.7	4.8 ± 0.4	3.3 ± 1.0	4.5 ± 0.6**
κ	0.86	0.90	0.94	0.94
Secondary				
R1	3.9 ± 0.8	3.9 ± 0.8	2.0 ± 1.0	3.2 ± 1.3**
R2	3.9 ± 0.7	3.9 ± 0.8	2.0 ± 1.0	3.1 ± 1.3**
κ	0.87	0.88	0.90	0.95
ACoA				
R1	3.5 ± 1.4	3.4 ± 1.5	3.3 ± 1.4	3.5 ± 1.4*
R2	3.5 ± 1.4	3.4 ± 1.5	3.2 ± 1.3	3.5 ± 1.5*
κ	0.90	0.91	0.87	0.86
PCoA				
R1	3.6 ± 1.0	3.7 ± 0.9	3.5 ± 1.0	4.0 ± 0.9**
R2	3.6 ± 1.1	3.7 ± 1.0	3.4 ± 1.0	4.1 ± 0.9**
κ	0.89	0.95	0.90	0.89

Table 3. Averaged Readers' Scores of TOF and Sparse TOF (continued)

Parameter	TOF and Sparse TOF with Same Resolution		TOF and Sparse TOF with Same Scan Time	
	TOF	Sparse TOF	TOF	Sparse TOF
ICA				
R1	5.0 ± 0.0	5.0 ± 0.0	4.9 ± 0.3	5.0 ± 0.0*
R2	5.0 ± 0.0	5.0 ± 0.0	4.8 ± 0.4	5.0 ± 0.2*
κ	1.00	1.00	0.87	0.86
BA				
R1	5.0 ± 0.0	5.0 ± 0.0	4.9 ± 0.3	5.0 ± 0.0
R2	5.0 ± 0.0	5.0 ± 0.0	4.9 ± 0.3	5.0 ± 0.0
κ	1.00	1.00	0.84	1.00
Artifacts				
R1	4.6 ± 0.8	4.7 ± 0.6	4.2 ± 0.5	4.8 ± 0.5**
R2	4.6 ± 0.8	4.7 ± 0.6	4.2 ± 0.5	4.8 ± 0.5**
κ	0.92	0.89	0.93	0.89
Overall vessel visualization				
R1	5.0 ± 0.2	4.9 ± 0.6	4.4 ± 0.5	4.9 ± 0.3**
R2	4.9 ± 0.3	4.8 ± 0.6	4.3 ± 0.5	4.8 ± 0.4**
κ	0.78	0.79	0.85	0.87
Overall image quality				
R1	4.7 ± 0.6	4.9 ± 0.4	4.1 ± 0.5	4.8 ± 0.4**
R2	4.7 ± 0.7	4.8 ± 0.5	4.1 ± 0.5	4.7 ± 0.4**
κ	0.89	0.84	0.84	0.91

Sparse TOF compared with TOF (*$p < 0.05$, **$p < 0.01$). ACA = anterior cerebral artery, ACoA = anterior communicating artery, BA = basilar artery, ICA = internal carotid artery, MCA = middle cerebral artery, PCA = posterior cerebral artery, PCoA = posterior communicating artery
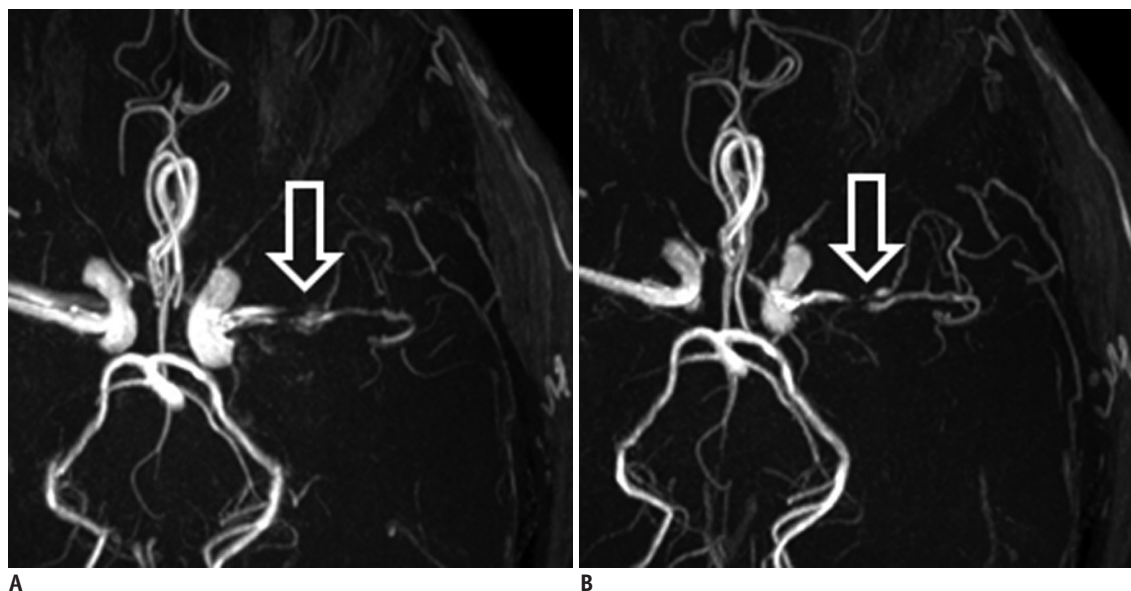

Fig. 1. Axial MIP images from conventional TOF (A) and sparse TOF (B) using same spatial resolution in 60-year-old man.
Display of lesion in left MCA is poorer on conventional TOF **(A)** because of motion artifacts (arrow). MCA = middle cerebral artery, MIP = maximum intensity projection, sparse TOF = TOF with sparse undersampling and iterative reconstruction, TOF = time-of-flight

Statistical Analysis

The statistical analysis was performed by using SPSS 19.0 (IBM Corp., Armonk, NY, USA). Numerical data are presented as the mean ± the standard deviation. The non-parametric Wilcoxon signed-rank test was used for qualitative comparisons between sparse and conventional TOF MRA. The paired t test was used for comparisons of CRs. Interobserver agreements for the delineation of arterial vessel segments,
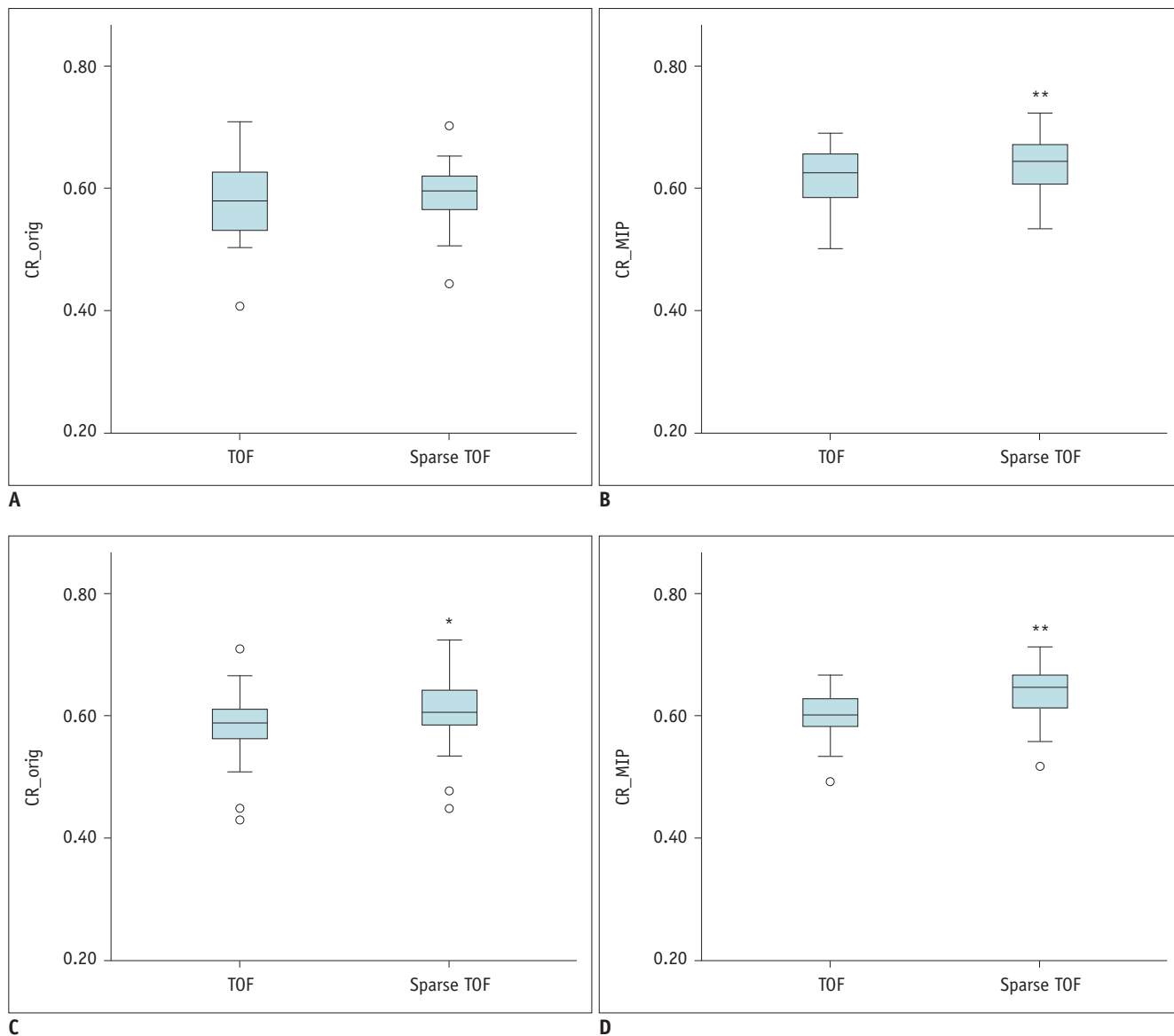
Fig. 2. Statistical analysis of CRs between conventional TOF and sparse TOF on original and MIP images.
A, B. CR shows no difference on original images but shows slight increase on MIP images for scanning-resolution-matched sparse TOF compared with that of conventional TOF (0.64 ± 0.05 vs. 0.61 ± 0.05, **$p < 0.001$). **C, D.** CR increased from 0.58 ± 0.06 to 0.60 ± 0.06 on original images (*$p < 0.05$) and from 0.59 ± 0.04 to 0.64 ± 0.04 on MIP images (**$p < 0.001$) on scanning-time-matched sparse TOF compared with conventional TOF. CR = contrast ratio, orig = original images

artifacts, overall vessel visualization, and overall image quality scores were calculated by using the kappa test (κ values of 0.00–0.20 were considered to indicate poor agreement; κ values of 0.21–0.40, fair agreement; κ values of 0.41–0.60, moderate agreement; κ values of 0.61–0.80, good agreement; and κ values of 0.81–1.00, excellent agreement). A p value less than 0.05 was considered to indicate statistical significance.

RESULTS

The acquisition and image reconstruction were successful for all 56 patients. Among them, five were diagnosed as having vessel stenoses, while the others presented healthy intracranial vasculatures.

When comparing sparse and conventional TOF MRA with similar spatial resolutions, sparse TOF showed comparable image quality regarding the delineation of vessel segments, artifacts, overall vessel visualization, and overall image quality compared with conventional TOF (Table 3). Even
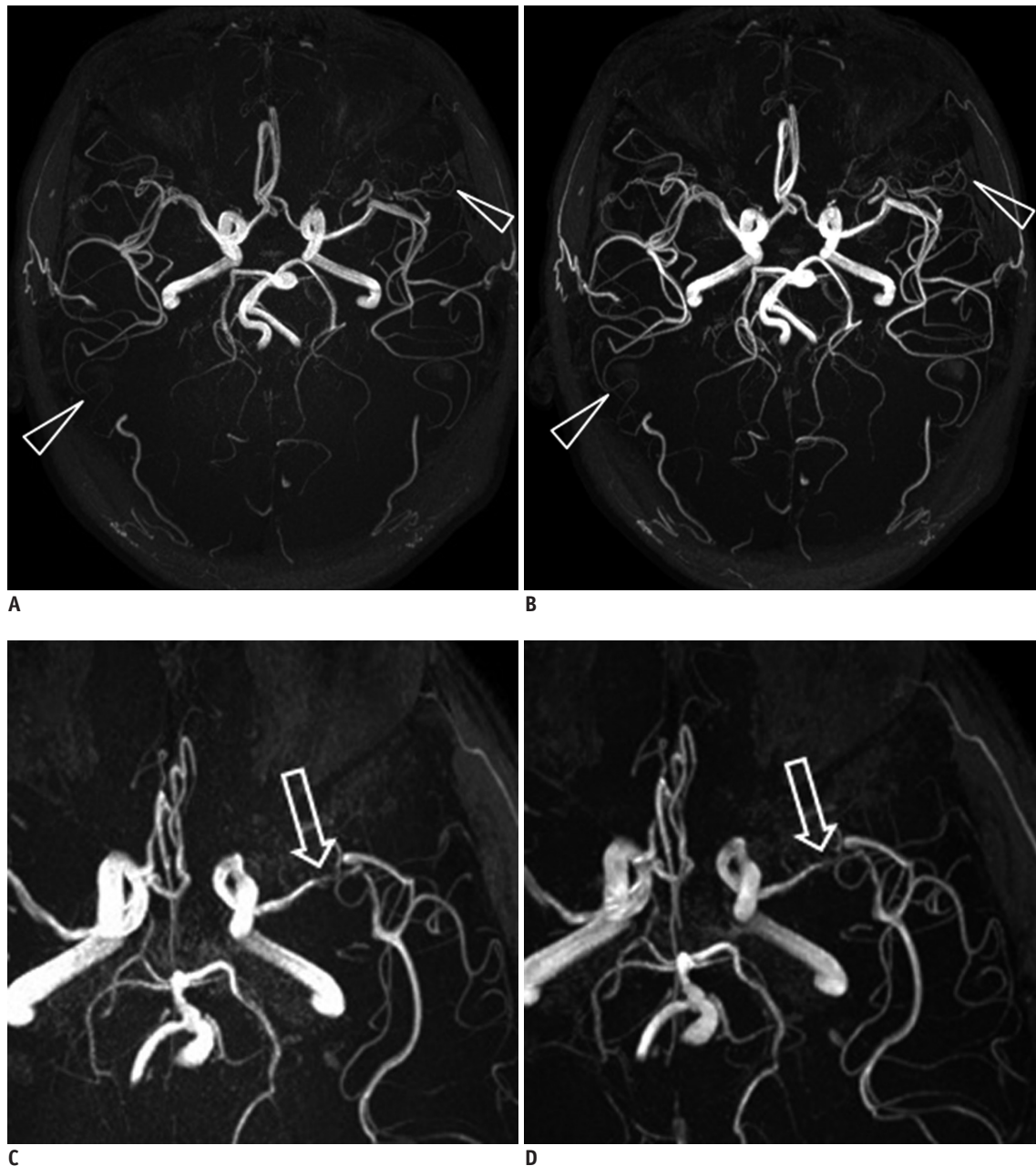
Fig. 3. Axial MIP images from conventional TOF (A, C) and sparse TOF (B, D) using same scanning time in two patients.
A and **B** are from 46-year-old woman and **C** and **D** are from 70-year-old man with left MCA stenosis. Delineation of fine vessels is better with sparse TOF than conventional TOF (arrowheads). Moreover, display of vessel stenosis is clearer with sparse TOF than with conventional TOF (arrows).

in patients with poor compliance, motion artifacts were reduced in sparse TOF MRA (Fig. 1). In the quantitative analysis, the CRs showed no difference on the original images, but a slight increase was observed on MIP images for sparse TOF compared with conventional TOF (0.64 ± 0.05 vs. 0.61 ± 0.05, $p < 0.001$) (Fig. 2A, B).

As shown in Figure 3 for two representative datasets, the presence of artifacts, overall vessel visualization, and overall image quality were superior for sparse TOF when compared with conventional TOF with a similar scanning time. The delineation of vessel segments was also significantly increased in the main branches of the ACA, ACoA, PCoA, and ICA, the primary sub-branches of the ACA and PCA, and the secondary sub-branches of the ACA, MCA, and PCA (Table 3). Comparing sparse TOF with conventional TOF, the CR increased from 0.58 ± 0.06 to 0.60 ± 0.06 on the original images ($p < 0.05$) and from 0.59 ± 0.04 to 0.64 ± 0.04 on the MIP images ($p < 0.001$) (Fig. 2C, D).

Good-to-excellent interobserver agreement (κ values: 0.65–1.00) was obtained between the two radiologists regarding the delineation of arterial vessel segments, artifacts, overall vessel visualization, and overall image quality scores (Table 3).

DISCUSSION

In the present work, we evaluated a sparse TOF technique for the acceleration of data acquisition in the context of non-contrast-enhanced MRA integrated into a clinical scanner. The performance of sparse TOF with a net acceleration factor of up to 5 was evaluated and compared with that of conventional TOF. Based on comparisons with protocols using either a matched spatial resolution or matched scanning time, we found that the sparse TOF technique reduced the acquisition time by 40% while maintaining comparable image quality and achieved superior results in cases with matched scanning times between sparse and conventional TOF.

High spatial resolution is essential for the detection of small-vessel disease and aids doctors in discovering more vascular lesions and developing the treatment plan. The major drawback of conventional TOF MRA with high resolution is the long acquisition time, which also renders the resulting images susceptible to artifacts due to any type of motion. Conventional parallel imaging techniques, such as mSENSE and GRAPPA, can reduce the acquisition time by reducing the number of phase encoding steps. It is well known that higher acceleration factors can be achieved with more coil elements because the parallel imaging technique needs the coil elements' phase information to reconstruct the final images. In addition, a higher SNR can be obtained with more elements (25). Therefore, it is useful to perform TOF MRA with multiple coil elements. However, an acceleration factor of 2–3 is feasible with conventional TOF. A further increase in parallel factors results in significant SNR loss (26, 27). Compared with conventional TOF, the acceleration factor of sparse TOF was affected by the undersampling factor. Furthermore, the SNRs of reconstructed images from sparse TOF were also associated with undersampling and the iteration steps in the image reconstruction (12). Therefore, compared with conventional TOF, sparse TOF can use a higher acceleration factor with the same phased array coils. In our study, as conventional TOF and sparse TOF were obtained using the same 20-channel head coil, the effect of the coil elements

on the SNR would be the same, but the acceleration factor can be set higher in sparse TOF than in conventional TOF.

Sparse MRI approaches matching the basic requirement for both high acceleration factors and high SNR have been reported previously for contrast-enhanced MRA, whole-heart coronary MRA, peripheral TOF MRA (9, 12, 14, 15, 28), as well as intracranial TOF MRA (16, 17). However, because of the long reconstruction times and/or limited availability of inline reconstruction algorithms at present, the clinical evaluation of compressed-sensing MRI techniques remains limited. In this work, we used a recently reported sparse TOF technique that was fully integrated on a clinical scanner for the clinical evaluation of 56 patients.

Our results demonstrated that with a net acceleration factor of 5, sparse TOF could acquire MRA images with a voxel size of 0.3 x 0.3 x 0.4 mm³ within 4 minutes with much higher image quality than that of conventional TOF with a similar scanning time. The reconstruction time for sparse TOF was 4–5 minutes for each patient on our MRI scanner. By using more advanced graphics processing units, a reduction in reconstruction time is possible. In our protocol, T_1-weighted imaging, T_2-weighted imaging, T_2 fluid-attenuated inversion recovery, and diffusion-weighted imaging were acquired for clinical diagnosis in addition to TOF MRA. These sequences can be performed while the MRI scanner is simultaneously reconstructing the sparse TOF MRA. Therefore, it does not increase the total scanning time.

By using the same spatial resolution for both sequences, our results demonstrated that sparse TOF presented comparable image quality to that of conventional TOF with a remarkable reduction in scanning time. The overall image quality, overall vessel visualization, and presence of artifacts were similar for both sequences, and no significant differences were shown in the delineation of vessel segments. These results are consistent with those of previous reports (18), which found that cerebral aneurysms were visible on sparse TOF accelerated by a factor of 5 with equivalent quality to that of traditional TOF, while the scanning time of sparse TOF accelerated by a factor of 5 was shorter than that of conventional TOF. In our study, the CR in the M1 segment of the MCA showed no significant differences between the two techniques on the original images but showed a slight increase on the MIP images. This was caused mainly by motion artifacts in patients with poor compliance when using conventional TOF MRA as the acquisition time was longer.

To match the scanning time, the slice thickness was

increased for conventional TOF compared with sparse TOF with a higher acceleration factor, as the acceleration factor could not be increased to guarantee an adequate SNR. Considering this condition, thicker slices were needed for conventional MRA to obtain the same coverage and in-plane resolution as those of sparse TOF MRA. The scores of large-diameter vessels, including the main branches of the MCA, PCA, and BA, did not show any difference between the sequences. However, the delineation of small vessels was improved when using sparse TOF, which might be due to the volume averaging effect and iterative reconstruction. Another important reason might be a result of the iterative reconstruction. The process of image reconstruction using an iterative reconstruction algorithm can also be considered for image denoising. With an optimized regularization weighting factor, a good balance between the noise level and image details can be achieved (12), resulting in increased contrast of the small vessels. This result highlighted the usefulness of sparse TOF in the diagnoses of stenosis and small-vessel occlusion. Although the ratings of the main branches did not show any difference, a more detailed analysis using the CR showed that the CR of vessels increased significantly on the original and MIP images.

Our study has limitations. First, the acceleration factor, regularization, and number of iterations of the protocols were fixed to compare the two methods. Further assessment of image quality with regard to these parameters should be addressed. Second, the subjects in this study were mostly patients without lesions in vessels; thus, diagnostic accuracies were not compared in the current study.

In this study, sparse TOF with a variable-density Poisson disk sampling pattern and iterative reconstruction was successfully integrated on a standard clinical MR scanner. The total acquisition time was significantly reduced without any tradeoff in image quality.

Conflicts of Interest
The authors have no financial conflicts of interest.

ORCID
Jiayu Sun
  https://orcid.org/0000-0002-9552-6720
Hehan Tang
  https://orcid.org/0000-0002-3882-4270

REFERENCES

1. Keller PJ, Drayer BP, Fram EK, Williams KD, Dumoulin CL, Souza SP. MR angiography with two-dimensional acquisition and three-dimensional display. Work in progress. *Radiology* 1989;173:527-532
2. Miyazaki M, Akahane M. Non-contrast enhanced MR angiography: established techniques. *J Magn Reson Imaging* 2012;35:1-19
3. Wheaton AJ, Miyazaki M. Non-contrast enhanced MR angiography: physical principles. *J Magn Reson Imaging* 2012;36:286-304
4. Laub GA. Time-of-flight method of MR angiography. *Magn Reson Imaging Clin N Am* 1995;3:391-398
5. Cho YD, Kim KM, Lee WJ, Sohn CH, Kang HS, Kim JE, et al. Time-of-flight magnetic resonance angiography for follow-up of coil embolization with enterprise stent for intracranial aneurysm: usefulness of source images. *Korean J Radiol* 2014;15:161-168
6. Papke K, Brassel F. Modern cross-sectional imaging in the diagnosis and follow-up of intracranial aneurysms. *Eur Radiol* 2006;16:2051-2066
7. Pruessmann KP, Weiger M, Scheidegger MB, Boesiger P. SENSE: sensitivity encoding for fast MRI. *Magn Reson Med* 1999;42:952-962
8. Griswold MA, Jakob PM, Heidemann RM, Nittka M, Jellus V, Wang J, et al. Generalized autocalibrating partially parallel acquisitions (GRAPPA). *Magn Reson Med* 2002;47:1202-1210
9. Lustig M, Donoho D, Pauly JM. Sparse MRI: the application of compressed sensing for rapid MR imaging. *Magn Reson Med* 2007;58:1182-1195
10. Donoho DL. Compressed sensing. *IEEE Transactions on Information Theory* 2006;52:1289-1306
11. Liang D, Liu B, Wang J, Ying L. Accelerating SENSE using compressed sensing. *Magn Reson Med* 2009;62:1574-1584
12. Stalder AF, Schmidt M, Quick HH, Schlamann M, Maderwald S, Schmitt P, et al. Highly undersampled contrast-enhanced MRA with iterative reconstruction: integration in a clinical setting. *Magn Reson Med* 2015;74:1652-1660
13. Rapacchi S, Han F, Natsuaki Y, Kroeker R, Plotnik A, Lehrman E, et al. High spatial and temporal resolution dynamic contrast-enhanced magnetic resonance angiography using compressed sensing with magnitude image subtraction. *Magn Reson Med* 2014;71:1771-1783
14. Hutter J, Grimm R, Forman C, Hornegger J, Schmitt P. Highly undersampled peripheral time-of-flight magnetic resonance angiography: optimized data acquisition and iterative image reconstruction. *MAGMA* 2015;28:437-446
15. Forman C, Piccini D, Grimm R, Hutter J, Hornegger J, Zenge MO. High-resolution 3D whole-heart coronary MRA: a study on the combination of data acquisition in multiple breath-holds and 1D residual respiratory motion compensation. *MAGMA* 2014;27:435-443
16. Natsuaki Y, Bi X, Zenge M, Speier P, Schmitt P, Laub G. Time-

Of-Flight with sparse undersampling (TOFu): towards practical MR applications of the compressed sensing. *Proc. Intl. Soc. Mag. Reson. Med* 2014;22:941

17. Stalder AF, Natsuaki Y, Schmidt M, Bi X, Zenge MO, Nadar M, et al. *Accelerating TOF MRA in clinical practice using sparse MRI with variable poisson density sampling*. International Society for ISMRM Magnetic Resonance in Medicine: ONE community for Clinicians and scientists 23rd annual meeting;2015 May 30-June 5; Toronto, Canada

18. Fushimi Y, Okada T, Kikuchi T, Yamamoto A, Okada T, Yamamoto T, et al. Clinical evaluation of time-of-flight MR angiography with sparse undersampling and iterative reconstruction for cerebral aneurysms. *NMR Biomed* 2017;30:3774

19. Yamamoto T, Fujimoto K, Okada T, Fushimi Y, Stalder AF, Natsuaki Y, et al. Time of Flight magnetic resonance angiography with sparse undersampling and iterative reconstruction: comparison with conventional parallel imaging for accelerated imaging. *Invest Radiol* 2016;51:372-378

20. Fushimi Y, Fujimoto K, Okada T, Yamamoto A, Tanaka T, Kikuchi T, et al. Compressed sensing 3-dimensional time-of-flight magnetic resonance angiography for cerebral aneurysms: optimization and evaluation. *Invest Radiol* 2016;51:228-235

21. Akasaka T, Fujimoto K, Yamamoto T, Okada T, Fushimi Y, Yamamoto A, et al. Optimization of regularization parameters in compressed sensing of magnetic resonance angiography: can statistical image metrics mimic radiologists' perception? *PLoS One* 2016;11:e0146548

22. Kayvanrad M, Lin A, Joshi R, Chiu J, Peters T. Diagnostic quality assessment of compressed sensing accelerated magnetic resonance neuroimaging. *J Magn Reson Imaging* 2016;44:433-444

23. Beck A, Teboulle M. A fast iterative shrinkage-Thresholding algorithm for linear inverse problems. SIAM J. *Imaging Sci* 2009;2:183–202

24. Wrede KH, Johst S, Dammann P, Özkan N, Mönninghoff C, Kraemer M, et al. Improved cerebral time-of-flight magnetic resonance angiography at 7 Tesla – Feasibility study and preliminary results using optimized venous saturation pulses. *PLoS ONE* 2014;9:e106697

25. de Zwart JA, Ledden PJ, van Gelderen P, Bodurka J, Chu R, Duyn JH. Signal-to-noise ratio and parallel imaging performance of a 16-channel receive-only brain coil array at 3.0 Tesla. *Magn Reson Med* 2004;51:22-26

26. Lin FH, Kwong KK, Belliveau JW, Wald LL. Parallel imaging reconstruction using automatic regularization. *Magn Reson Med* 2004;51:559-567

27. Michaely HJ, Herrmann KA, Kramer H, Dietrich O, Laub G, Reiser MF, et al. High-resolution renal MRA: comparison of image quality and vessel depiction with different parallel imaging acceleration factors. *J Magn Reson Imaging* 2006;24:95-100

28. Forman C, Piccini D, Grimm R, Hutter J, Hornegger J, Zenge MO. Reduction of respiratory motion artifacts for free-breathing whole-heart coronary MRA by weighted iterative reconstruction. *Magn Reson Med* 2015;73:1885-1895